



F-53B disrupts energy metabolism by inhibiting the V-ATPase-AMPK axis in neuronal cells

Yue Zhang^{a,b,c}, Tingting Li^{a,b,c}, Xueman Ding^{a,b,c}, Li Liu^{a,b,c},
Runjiang Ma^{a,b,c}, Wenqi Qin^{a,b,c}, Chulin Yan^{a,b,c}, Chun Wang^{a,b,c},
Jingjing Zhang^{a,b,c}, Mulatibieke Keerman^{a,b,c,*}, Qiang Niu^{a,b,c,*}

^a Key Laboratory for Prevention and Control of Emerging Infectious Diseases and Public Health Security, the Xinjiang Production and Construction Corps, School of Medicine, Shihezi University, Shihezi, PR China

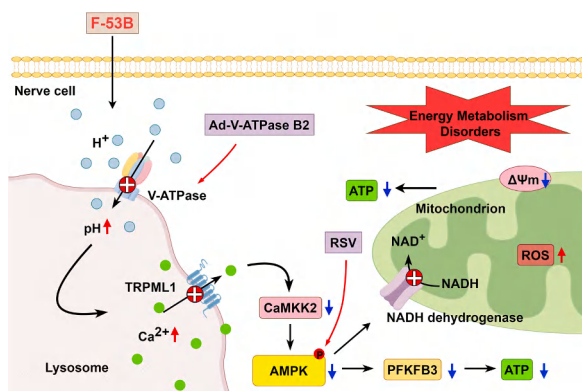
^b Key Laboratory of Xinjiang Endemic and Ethnic Diseases (Ministry of Education), School of Medicine, Shihezi University, Shihezi, Xinjiang, PR China

^c NHC Key Laboratory of Prevention and Treatment of Central Asia High Incidence Diseases (First Affiliated Hospital, School of Medicine, Shihezi University), PR China

HIGHLIGHTS

- F-53B disrupts neuronal energy metabolism via V-ATPase-AMPK axis.
- V-ATPase overexpression rescues lysosomal Ca^{2+} efflux and AMPK activity.
- RSV activates AMPK, restoring energy metabolism in F-53B-treated neurons.

GRAPHICAL ABSTRACT



ARTICLE INFO

Keywords:

F-53B
Neurotoxicity
V-ATPase-AMPK axis
Mitochondrial energy metabolism
Lysosomal dysfunction

ABSTRACT

6:2 chloro-polyfluorooctane ether sulfonate (F-53B) is considered neurotoxic, but its mechanisms remain unclear. This study aimed to investigate the toxic effects of F-53B on neuronal cells, focusing on the role of the V-ATPase-AMPK axis in the mechanism of abnormal energy metabolism. Mouse astrocytes (C8-D1A) and human neuroblastoma cells (SH-SY5Y) exposed to F-53B were used as *in vitro* models. Our findings demonstrated that F-53B inhibited the expression of V-ATPase B2 and reduced V-ATPase activity, leading to an increase in lysosomal pH, decreased expression of TRPML1, and lysosomal Ca^{2+} accumulation. In turn, led to reduced the expression of CaMKK2 and phosphorylated AMPK (p-AMPK). Ultimately, mitochondria were damaged, evidenced by increased mitochondrial reactive oxygen species, mitochondrial membrane potential, and impaired mitochondrial oxidative phosphorylation, as shown by reduced NDUFS1 expression and diminished respiratory chain complex I activity. F-53B reduced the expression of the key glycolytic protein PFKFB3. Notably, V-ATPase B2 overexpression indirectly activates AMPK. Furthermore, resveratrol, an AMPK agonist, alleviates mitochondrial

* Correspondence to: Department of Preventive Medicine, School of Medicine, Shihezi University, North 2th Road, Shihezi, Xinjiang 832000, PR China.

E-mail addresses: 464174936@qq.com (M. Keerman), niuqiang@shzu.edu.cn (Q. Niu).

<https://doi.org/10.1016/j.jhazmat.2025.137111>

Received 14 October 2024; Received in revised form 20 December 2024; Accepted 2 January 2025

Available online 4 January 2025

0304-3894/© 2025 Elsevier B.V. All rights are reserved, including those for text and data mining, AI training, and similar technologies.

dysfunction and increases ATP production by promoting the recovery of mitochondria and glycolytic pathways. These findings elucidate a novel mechanism by which F-53B induces neurotoxicity through the V-ATPase-AMPK axis, and indicate V-ATPase and AMPK as potential therapeutic targets.

1. Introduction

Perfluorooctane sulfonate (PFOS) has been classified as a persistent organic pollutant under the Stockholm Convention[1]. In China, PFOS was also included in the *List of New Pollutants for Priority Control (2023 Edition)*, which came into effect on March 1, 2023. As the use of PFOS has been severely restricted, one of its main substitutes, 6:2 chloro-polyfluorooctane ether sulfonate (6:2 Cl-PFESA, also known as F-53B), is becoming more widely used[2]. Research has shown that F-53B is present in various natural environments, including surface water[3], sewage sludge[4] and atmosphere[5]. A survey conducted in South Korea revealed an increasing trend of F-53B levels in black-tailed gull eggs from 2012 to 2018[6]. Additionally, F-53B has been detected in marine mammals in Greenland[7]. Toxicity tests using zebrafish revealed that F-53B is moderately toxic (LC50–96h, 15.5 mg/L) and not easily degradable[8]. An epidemiological study in China found that nearly 80 % of human blood samples contained F-53B[9]. In some cases, such as in Chinese metal plating workers, concentrations were as high as 5040 ng/mL, with an elimination half-life of 15.3 years[10]. These findings indicate that F-53B contamination is widespread and accumulates in living organisms, highlighting the need for greater attention to its potential risks to human health.

Among the many targets of environmental pollutants, the nervous system is particularly sensitive. F-53B has been shown to cross the blood-cerebrospinal fluid barrier and accumulate in cerebrospinal fluid [11]. A cross-sectional study found a significant negative correlation between the concentration of F-53B in newborns' cerebrospinal fluid and their head circumference[12]. Animal studies further revealed that F-53B disrupts the expression of neural marker genes and affects the morphology of differentiated cells during early neural development[13]. Notably, F-53B was found to potentially have stronger toxic effects[9]. Neurons, as the basic structural and functional units of the nervous system, are non-regenerative cells that cannot regenerate once they die. Therefore, more studies are needed to reveal the mechanism of F-53B toxicity to the nervous system.

Despite making up only 2 % of the body's weight, the brain accounts for 20 % of its energy consumption. Mitochondria, the primary sites of ATP production within cells, are essential for the proper functioning of nerve cells[14]. Adenosine 5'-monophosphate (AMP)-activated protein kinase (AMPK) is a key regulator of cellular energy metabolism and mitochondrial homeostasis, playing a crucial role in maintaining overall energy balance. When activated, AMPK positively regulates pathways that restore ATP levels while inhibiting those that lead to ATP depletion [15]. Mitochondrion, as the "power plant" of cells, produces ATP through processes including mitochondrial respiratory chain complexes I-IV, ATP synthase, cytochrome c, and ubiquinone[16]. Additionally, glycolysis also produces ATP, helping to maintain essential cellular metabolism and function.

An animal study revealed that PFOS inhibited the AMPK/mTOR/autophagy signaling pathway, leading to hepatic lipid accumulation [17]. A cellular study showed that PFOS impaired trophoblast cells by reducing ATP levels, compromising mitochondrial function, and inhibiting cellular respiration[18]. Furthermore, Nie et al.[19] demonstrated that F-53B promoted the generation of reactive oxygen species and induced apoptosis by disrupting mitochondrial structure and function. Given the central role of AMPK in mitochondrial energy metabolism and the potential for F-53B to trigger mitochondrial dysfunction, the role of AMPK in this process urgently requires further investigation. Lysosomes also play a critical role in maintaining intracellular homeostasis, particularly as the main reservoirs of calcium ions (Ca^{2+}), which are

essential for cellular energy metabolism and serve as important signaling molecules for AMPK activation. Li et al.[20] found that PFOS induced insulin resistance by activating autophagy and causing the accumulation of lysosomal and mitochondrial Ca^{2+} . Animal studies have revealed that exocytosed lysosomal Ca^{2+} can indirectly activate AMPK via calcium/calmodulin-dependent protein kinase kinase 2 (CaMKK2) [21]. Transient receptor potential mucolipid protein 1 (TRPML1), located on the lysosomal membrane, regulates Ca^{2+} efflux, and its expression is influenced by lysosomal pH[22]. Lysosomal pH, in turn, is regulated by H^+ -ATPase (V-ATPase), which helps maintain lysosomal homeostasis by creating the necessary microenvironment. Clearly, V-ATPase is the initiating factor in this complex process, regulating cellular energy metabolism by modulating lysosomal pH, which controls lysosomal Ca^{2+} efflux and ultimately affects AMPK activity, forming a crucial signaling axis.

Energy homeostasis is critical for the normal function of neuronal cells, combined with the available evidence, we hypothesize that the V-ATPase-AMPK signaling axis plays a key role in regulating energy metabolism in neuronal cells. To address this, we used mouse astrocytes (C8-D1A) and human neuroblastoma (SH-SY5Y) cells as *in vitro* models. As well as we used overexpression of V-ATPase B2 and resveratrol (RSV, a natural AMPK activator[23,24]) to target V-ATPase and AMPK, respectively. We aimed to explore the role of the V-ATPase-AMPK signaling axis in F-53B-induced energy metabolism disorders and neurotoxicity, and to provide valuable scientific insights for the prevention and treatment of F-53B-induced neurotoxicity.

2. Materials and methods

2.1. Antibodies, reagents, and chemicals

F-53B was generously provided by Professor Wenqing Tu from the School of Land Resources and Environment, Jiangxi Agricultural University, China. Resveratrol (RSV, CAS 501–36–0) was obtained from Solarbio (China). Both F-53B and RSV were dissolved in dimethyl sulfoxide (DMSO) to ensure solubility, with the concentration of DMSO < 0.1 % (v/v) in all experimental groups. V-ATPase B2 antibodies were purchased from Santa Cruz Biotechnology (USA), and TRPML1 antibodies were obtained from Thermo Fisher (USA). Acidified adenosine monophosphate-activated protein kinase alpha 1 (PRKAA1/AMPK α 1) antibodies were purchased from Boster Biotech (China), while phosphorylated AMPK (p-PRKAA1/p-AMPK α 1, T172) antibodies were obtained from Beyotime (China). Additional antibodies, including CaMKK2 (11549–1-AP), 6-phosphofructo-2-kinase/fructose-2,6-bisphosphatase 3 (PFKFB3) (13763–1-AP), recombinant NADH dehydrogenase ubiquinone Fe-S protein 1 (NDUFS1) (12444–1-AP), poly (ADP-ribose) polymerase (PARP) (13371–1-AP) and glyceraldehyde 3-phosphate dehydrogenase (GAPDH) (10494–1-AP), were provided by Proteintech (USA).

The Cell Counting Kit-8 (CCK-8, BS350B) was acquired from Biosharp (China) and LysoSensor™ Yellow/Blue DND-160 (PDMPO) was obtained from Yeasen (China). The V-ATPases ELISA kit was supplied by Huabang Bio-Technology Co., Ltd. (China), and Fluo-3 AM (C5092) was acquired from APEX-BIO (USA). Mito Tracker Green (C1048) and the ATP assay kit (S0027) were both purchased from Beyotime (China), while MitoSox Red (2411520) was obtained from Invitrogen (USA). LysoTracker Red (L8010), the mitochondrial membrane potential assay kit (JC-1) (M8650), and the mitochondrial respiratory chain complex I activity assay kit (BC0515) were sourced from Solarbio (China). The recombinant adenovirus plasmid expressing V-ATPase B2 was provided

by WZ Biosciences Inc. (China).

2.2. Cell culture and treatment

The nervous system consists mainly of neurons and glial cells. SH-SY5Y cells are morphologically, neurochemically and electrophysiologically characterized as similar to neurons [25,26], and astrocytes are the largest of the glial cells and are associated with energy metabolism [27,28]. Therefore, both were chosen as *in vitro* models for F-53B exposure. Mouse astrocytes (C8-D1A, CL-0506) were supplied by Procell (China), while human neuroblastoma (SH-SY5Y) cells were obtained from the Typical Cultures Depository (USA). Both cell lines were cultured in Dulbecco's modified Eagle's medium (DMEM) containing 10 % fetal bovine serum (FBS) and 1 % penicillin-streptomycin in a humidified environment at 37°C with 5 % CO₂. The concentrations of F-53B [10,13,19] were determined based on a combination of relevant literature and experimental CCK-8 results (Figure. S1A, B). Once the cells reached 70 %–80 % confluence in the culture flasks or plates, they were treated with 0, 2.5, 5.0, or 10.0 μM F-53B for 24 hours. C8-D1A cells were infected with a recombinant adenoviral plasmid expressing V-ATPase B2 (Ad-V-ATPase B2) at a multiplicity of infection (MOI) of 400, and SH-SY5Y cells were infected at an MOI of 300. After 24 hours of infection, the cells were treated with 10 μM F-53B for an additional 24 hours. RSV treatment dose and duration were determined according to the relevant literature [29–31] and CCK-8 results together (Figure. S1E, F). Additionally, C8-D1A cells were pre-treated with 10 μM RSV, and SH-SY5Y cells with 5 μM RSV for 2 hours prior to the application of 10 μM F-53B.

2.3. Cell viability by CCK-8 assay

Cell viability was assessed using the Cell Counting Kit-8 (CCK-8) assay. Cells were seeded into 96-well plates, and the CCK-8 solution was prepared by mixing CCK-8 with basal medium (without FBS) at a 1:10 ratio. After incubating the cells for 0.5–2 hours, absorbance was measured at 450 nm using a microplate reader. Cell viability (%) was calculated based on the following formula: cell viability = (OD value (optical density) of the experimental group - OD value of the blank control group) / (OD value of the control group - OD value of the blank control group) × 100 %, with at least three independent experiments were performed.

2.4. Western blot

Proteins from C8-D1A and SH-SY5Y cells were extracted using RIPA lysis buffer. Phosphatase inhibitors were added to the lysate in equal proportion to PMSF to preserve phosphorylated proteins. The total protein concentration in the samples was determined using a BCA assay kit. Proteins were separated via sodium dodecyl sulfate-polyacrylamide gel electrophoresis and transferred onto polyvinylidene fluoride membranes. The membranes were blocked with 5 % skim milk at room temperature for 1.5 hours, followed by overnight incubation at 4°C with primary antibodies targeting V-ATPase B2 (1:100), TRPML1 (1:2000), PRKAA1/AMPKα1 (1:500), p-PRKAA1/ p-AMPKα1 (T172) (1:1000), CaMKK2 (1:1000), NDUFS1 (1:5000), PFKFB3 (1:3000), PARP (1:1000) and GAPDH (1:50000). The next day, the membranes were incubated with secondary antibodies (1:20,000) for 1.5 hours at room temperature. After washing the membranes three times with TBST, protein bands were visualized using an Enhanced Chemiluminescence reagent and captured using a Tanon-5200 Chemiluminescence Image Analysis System. Protein band intensities were quantified using the ImageJ software. Each band's density was adjusted to the control, and three independent experiments were carried out to ensure reproducibility.

2.5. Measurement of lysosomal pH

Cells were treated with 2 μM LysoSensor™ Yellow/Blue DND-160 for 30–60 minutes at 37°C. After treatment, the cells were washed three times with PBS, and fluorescence intensity was immediately observed using laser confocal microscopy (Nikon AX R, Japan) under light-protected conditions. Quantitative analysis was performed using the ImageJ software, with experiments repeated independently three times.

2.6. V-ATPase activity assay

Cell lysates were collected, and the supernatant was used for the assay. Test wells were prepared by adding 10 μL of the sample, 40 μL of sample dilution, and 100 μL of horseradish peroxidase-labeled detection antibody. The wells were sealed with a sealing film and incubated in a constant temperature oven for 60 minutes. After washing each well five times with a washing solution, 50 μL of substrate A and 50 μL of substrate B were added to each well and incubated for 15 minutes at 37°C, protected from light. Finally, 50 μL of termination solution was added to each well, and the OD value was measured at 450 nm within 15 minutes. Experiments were performed independently in triplicate.

2.7. Lysosomal Ca²⁺ assay

After treatment, cells were stained with LysoTracker Red diluted to 50 nM in serum-free medium to detect lysosomes. Ca²⁺ levels were measured by diluting Fluo-3 AM stock solution to 5 μM in serum-free medium. The cells were incubated with the dye for 30 minutes at 37°C, then washed with PBS. Fresh DMEM was added, and fluorescence intensity was immediately observed using laser confocal microscopy (Nikon AX R, Japan) under light-protected conditions. Quantitative analyses were conducted using the ImageJ software, with experiments performed independently three times.

2.8. Mitochondrial reactive oxygen species (mtROS) assay

Upon treatment, cells were incubated in DMEM containing 200 nM Mito Tracker Green for 30 minutes at 37°C. The cells were then washed with PBS and incubated in a working solution containing 5 μM MitoSox Red for 30 minutes at 37°C. After a single wash with PBS, fresh DMEM was added, and the fluorescence intensity of the cells was immediately observed using laser confocal microscopy (Nikon AX R, Japan) under light-protected conditions. Quantitative analyses were performed using the ImageJ software, with experiments repeated independently three times.

2.9. Mitochondrial membrane potential (MMP) assay

MMP levels were detected using the JC-1 probe. After treatment, C8-D1A and SH-SY5Y cells in the positive control group were gently washed with PBS, followed by the addition of 10 μM CCCP (Carbonyl cyanide 3-chlorophenylhydrazide), as a positive control for inducing a decrease in mitochondrial membrane potential. The cells were incubated at 37°C for 40 minutes. JC-1 staining working solution was then added to all groups and incubated at 37 °C for at least 30 minutes. After staining, the cells were gently rinsed three times with pre-cooled 1 × staining buffer, fresh DMEM was added, and the fluorescence intensity was immediately observed using laser confocal microscopy (Nikon AX R, Japan) in a light-protected environment. Quantitative analyses were performed using the ImageJ software, with experiments independently repeated three times.

2.10. Mitochondrial respiratory chain complex I (complex I, CI) activity assay

At least 5 million cells were collected for the assay. The relevant reagents were added to a 96-well UV plate according to the

manufacturer's instructions. Absorbance was measured at 340 nm every 10 seconds, with subsequent readings taken at 1 minute and 10 seconds. The activity of the samples was calculated based on recommended protein concentrations. Experiments were performed independently in triplicate.

2.11. Detection of ATP levels

ATP levels were measured using a 96-well plate. A total of 100 μ L of ATP assay working solution (ATP assay reagent: sample dilution = 1:4) was added to each well. After standing at room temperature for 3–5 minutes, 30 μ L of the sample was added to each well or assay tube and quickly mixed using a micropipette. The relative light units (RLU) were measured using the chemiluminescence function of a multifunctional enzyme labeler. At least three independent experiments were performed.

2.12. Statistical analysis

All data were analyzed using SPSS 26.0 software. Results were expressed as mean \pm standard deviation (SD). One-way ANOVA followed by Tukey's test was used for multiple comparisons. Statistical significance was set at $P < 0.05$.

3. Results

3.1. F-53B causes mitochondrial damage and reduces ATP levels in neuronal cells

The effects of F-53B exposure on mitochondrial function in C8-D1A and SH-SY5Y cells were assessed by measuring mtROS content and changes in mitochondrial membrane potential (MMP) via immunofluorescence. Compared to the control group, MitoSox Red fluorescence in both C8-D1A and SH-SY5Y cells increased significantly with higher F-53B doses, indicating an elevation in mtROS levels (Fig. 1A–C, $P < 0.05$). Additionally, as the dose of F-53B increased, the green fluorescence in both cell lines also intensified, suggesting a reduction in MMP (Fig. 1D, E, $P < 0.05$). Collectively, these findings indicate that mitochondrial function was impaired. Furthermore, ATP levels, measured using an assay kit, revealed that F-53B significantly reduced ATP levels in both C8-D1A and SH-SY5Y cells (Fig. 1F, G, $P < 0.05$). In addition, we detected the apoptotic protein PARP, and the WB results suggested that F-53B elevated PARP protein expression (Figure. S1C, D, $P < 0.05$).

3.2. F-53B exposure inhibits the expression of p-AMPK and energy metabolism pathways in neuronal cells

Our findings revealed that F-53B exposure inhibited the expression of p-AMPK in C8-D1A and SH-SY5Y cells compared to the control group (Fig. 2A, B, $P < 0.05$). Additionally, the expression levels of PFKFB3 and NDUFS1 proteins were also significantly reduced with increasing F-53B doses (Fig. 2A, C, D, $P < 0.05$). CI activity in both cell lines was further analyzed, and exposure to 10.0 μ M F-53B significantly inhibited CI activity compared to the control group (Fig. 2E, F, $P < 0.05$).

3.3. F-53B exposure increases lysosomal pH and inhibits V-ATPase B2 expression and V-ATPase activity in neuronal cells

Western blot analysis revealed that F-53B significantly inhibited the expression of V-ATPase B2 in both C8-D1A and SH-SY5Y cells compared to the control group (Fig. 3A, B, $P < 0.05$). Furthermore, V-ATPase activity, as measured by a V-ATPase activity kit, was significantly reduced in F-53B-treated cells (Fig. 3C, D, $P < 0.05$). Additionally, our findings revealed an elevation in lysosomal pH in F-53B-treated C8-D1A and SH-SY5Y cells (Fig. 3E, F, $P < 0.05$).

3.4. F-53B exposure inhibits TRPML1 expression and reduces lysosomal Ca^{2+} release in neuronal cells

F-53B exposure significantly inhibited TRPML1 expression in C8-D1A and SH-SY5Y cells in a dose-dependent manner, as detected by western blotting (Fig. 4A, B, $P < 0.05$). Similarly, CaMKK2 protein expression was also reduced with increasing F-53B doses in both cell lines (Fig. 4A, C, $P < 0.05$). Immunofluorescence analysis demonstrated that F-53B increased Ca^{2+} accumulation in lysosomes of C8-D1A and SH-SY5Y cells (Fig. 4D, E, $P < 0.05$).

3.5. V-ATPase B2 overexpression restores F-53B-induced reductions in V-ATPase B2 expression and V-ATPase activity and alleviates elevated lysosomal pH of neuronal cells

To investigate whether Ad-V-ATPase B2 could counteract the F-53B-induced elevation of lysosomal pH in C8-D1A and SH-SY5Y cells, we re-examined several key indicators. Compared to the F-53B-treated group (Ad-null + F-53B), the cotreatment group (Ad-V-ATPase B2 + F-53B) showed a statistically significant increase in V-ATPase B2 expression (Fig. 5A, B, $P < 0.05$). Moreover, V-ATPase activity in both C8-D1A and SH-SY5Y cells was significantly elevated in the cotreatment group compared to the F-53B-treated group (Fig. 5C, D, $P < 0.05$). Immunofluorescence analysis revealed that overexpression of V-ATPase B2 effectively restored the F-53B-induced elevation of lysosomal pH, as shown by the attenuation of blue fluorescence in the cotreatment group compared to the F-53B group (Fig. 5E, F, $P < 0.05$).

3.6. V-ATPase B2 overexpression alleviates F-53B-induced TRPML1 inhibition and restores lysosomal Ca^{2+} release, AMPK activity, and ATP levels in neuronal cells

To assess whether Ad-V-ATPase B2 could alleviate the energy metabolism impairment caused by F-53B in C8-D1A and SH-SY5Y cells, we re-examined several key indicators. Western blot analysis showed a significant increase in TRPML1 expression in the cotreatment group compared to the F-53B-treated group (Figure. 6 A, B, $P < 0.05$). Additionally, immunofluorescence analysis revealed a decrease in lysosomal Ca^{2+} accumulation in the cotreatment group, as indicated by a reduction in green fluorescence intensity compared to the F-53B group (Fig. 6D, F, $P < 0.05$), suggesting that Ad-V-ATPase B2 could mitigate the inhibition of lysosomal Ca^{2+} release caused by F-53B. Western blot results for CaMKK2 and p-AMPK protein expression showed a significant increase in both markers in the cotreatment group compared to the F-53B group (Fig. 6A, C, E, $P < 0.05$). Moreover, ATP levels were significantly elevated in the cotreatment group compared to the F-53B group (Fig. 6G, $P < 0.05$).

3.7. RSV alleviates F-53B-induced inhibition of p-AMPK expression and restores cellular energy metabolic pathways in neuronal cells

To determine if RSV could mitigate the F-53B-induced inhibition of energy metabolism in C8-D1A and SH-SY5Y cells, we evaluated relevant indicators. Western blot analysis revealed that RSV treatment increased the expression of p-AMPK, PFKFB3, and NDUFS1 proteins following F-53B exposure (Fig. 7A–D, $P < 0.05$). Additionally, RSV treatment significantly enhanced CI activity after F-53B exposure, as demonstrated by enzyme assay results (Fig. 7E, F, $P < 0.05$).

3.8. RSV relieves mitochondrial damage induced by F-53B and restores cellular ATP levels in neuronal cells

To explore whether RSV could mitigate F-53B-induced mitochondrial damage and restore ATP levels in C8-D1A and SH-SY5Y cells, we analyzed relevant indicators. Immunofluorescence detection of mtROS showed that red fluorescence was significantly reduced in the RSV + F-

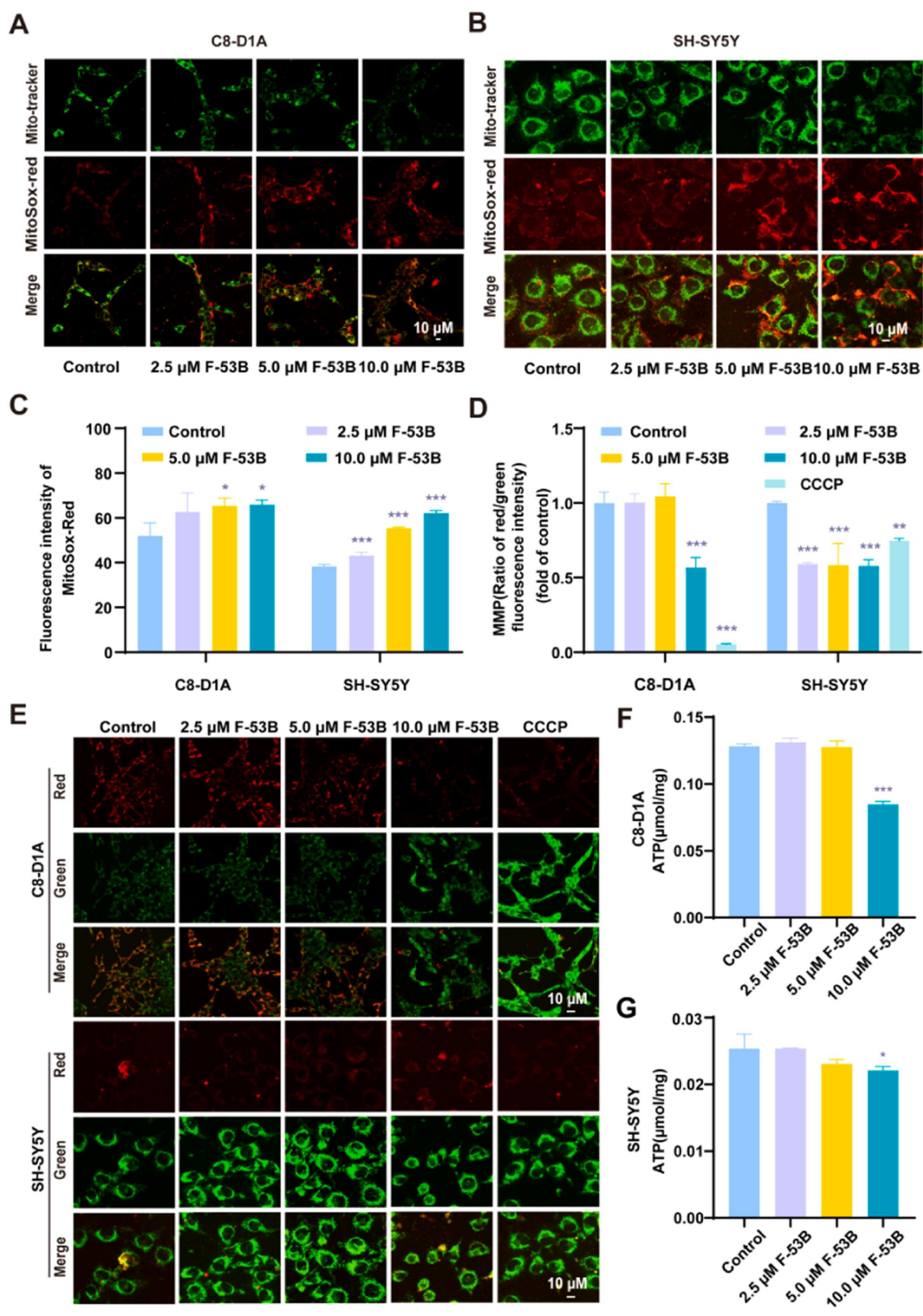


Fig. 1. F-53B causes mitochondrial damage and reduces ATP levels in neuronal cells. (A) Representative images of mtROS in C8-D1A cells. (B) Representative images of mtROS in SH-SY5Y cells. (C) Quantitative analyses of A and B. (D) Quantitative analyses of E. (E) Representative images of MMP in C8-D1A and SH-SY5Y cells. Red signals indicate JC-1 aggregate, green signals indicate JC-1 monomer, and CCCP is used as a positive control. (F) Plot of ATP levels in C8-D1A cells. (G) Plot of ATP levels in SH-SY5Y cells. Values represent the mean \pm SD (n = 3 replicates). * P < 0.05, ** P < 0.01, *** P < 0.005 compared with the control group.

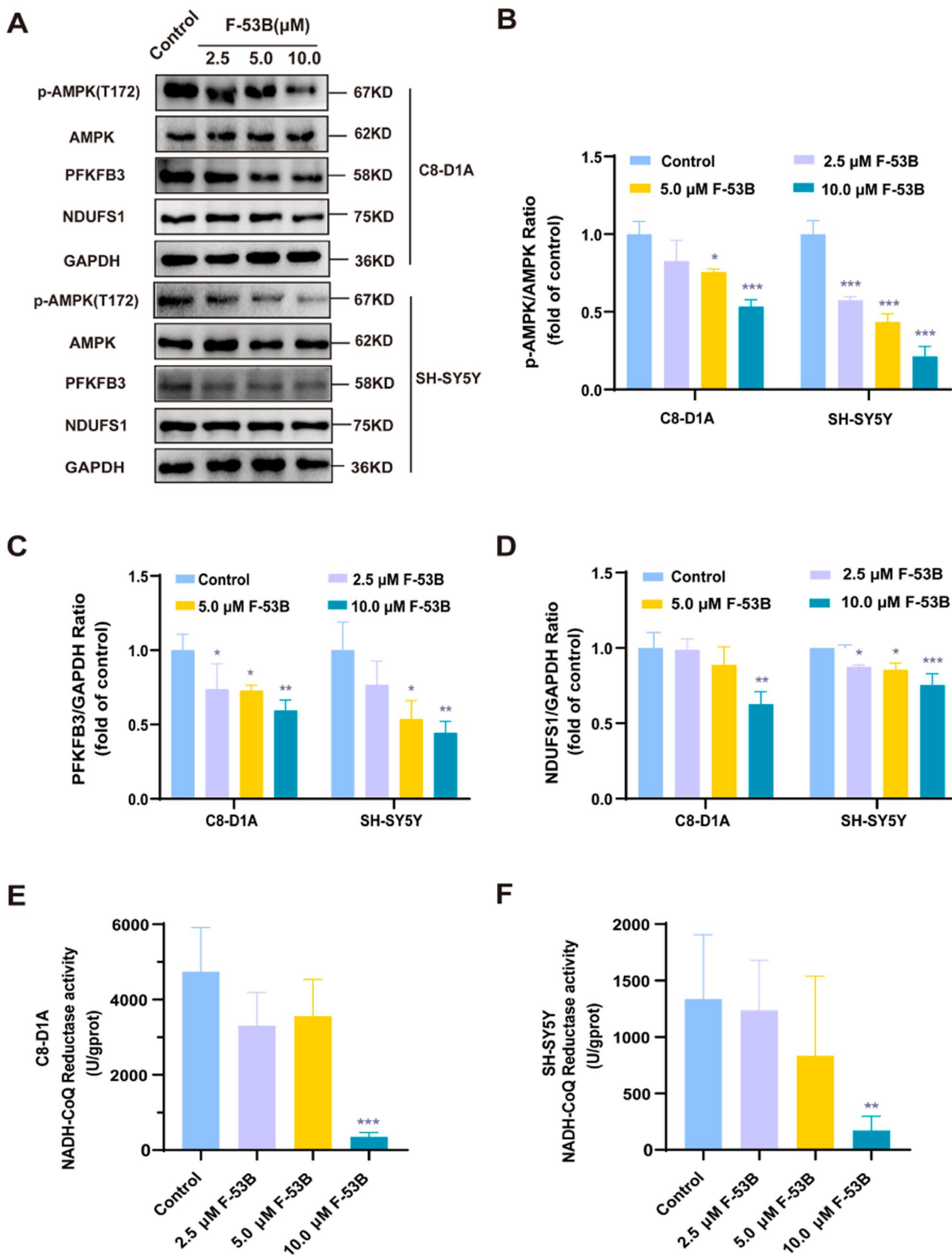


Fig. 2. F-53B exposure inhibits the expression of p-AMPK and energy metabolism pathways in neuronal cells. (A-D) Western blot and relative quantification of p-AMPK, AMPK, PFKFB3 and NDUFS1 in C8-D1A and SH-SY5Y cells. (E) Quantitative plot of the activity of CI in C8-D1A cells. (F) Quantitative plot of the activity of CI in SH-SY5Y cells. Values represent the mean ± SD (n = 3 replicates). * $P < 0.05$, ** $P < 0.01$, *** $P < 0.005$ compared with the control group.

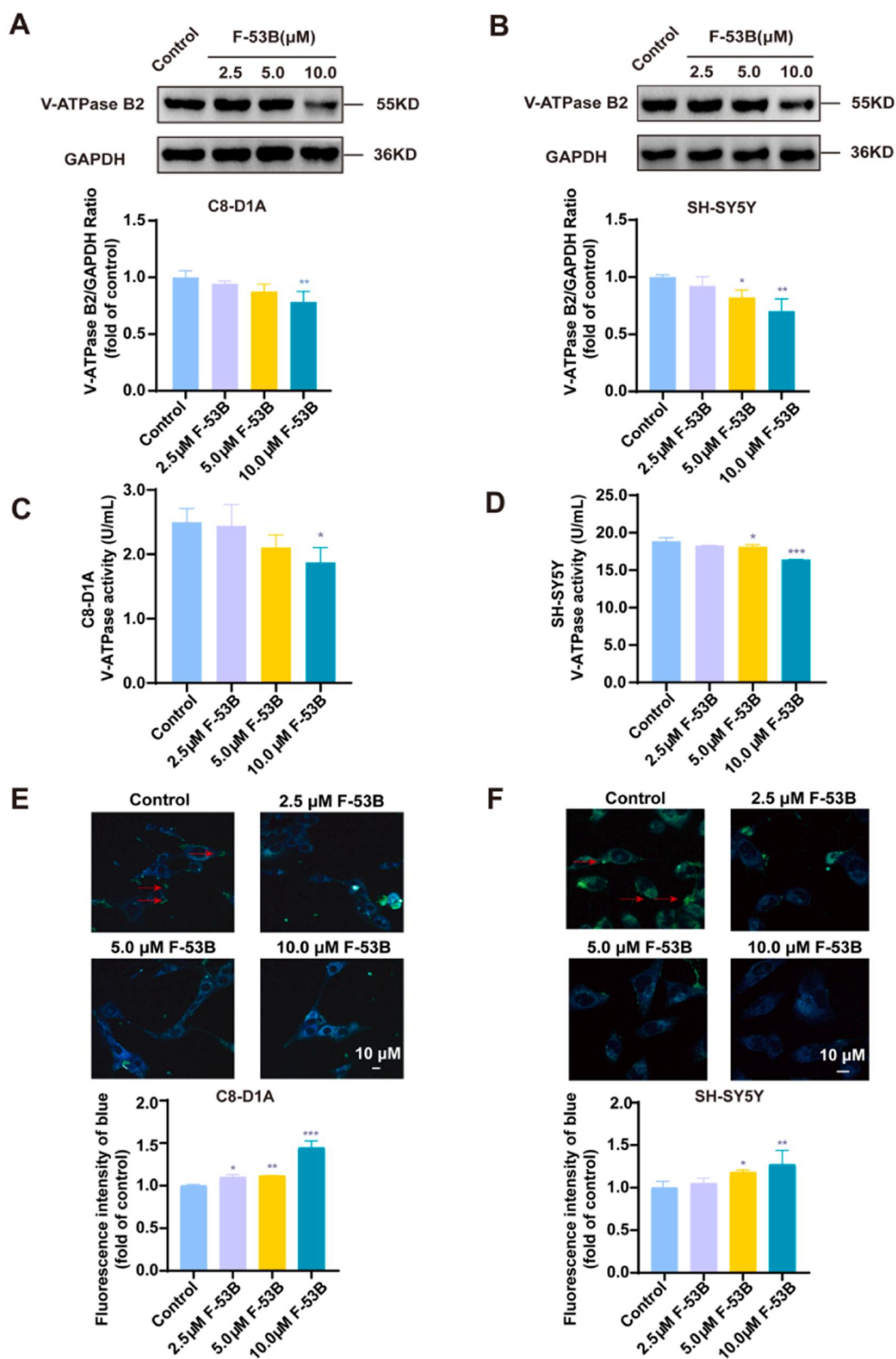


Fig. 3. F-53B exposure increases lysosomal pH and inhibits V-ATPase B2 expression and V-ATPase activity in neuronal cells. (A) Western blot and relative quantification of V-ATPase B2 in C8-D1A cells. (B) Western blot and relative quantification of V-ATPase B2 in SH-SY5Y cells. (C) Quantitative plot of V-ATPase complex activity in C8-D1A cells. (D) Quantitative plot of V-ATPase complex activity in SH-SY5Y cells. (E) Fluorescence assay and quantitative fluorescence analysis images of Lysosomal pH in C8-D1A cells. (F) Fluorescence assay and quantitative fluorescence analysis images of Lysosomal pH in SH-SY5Y cells. The red arrow denotes the acidic portion of the lysosomal pH. Values represent the mean \pm SD ($n = 3$ replicates). * $P < 0.05$, ** $P < 0.01$, *** $P < 0.005$ compared with the control group.

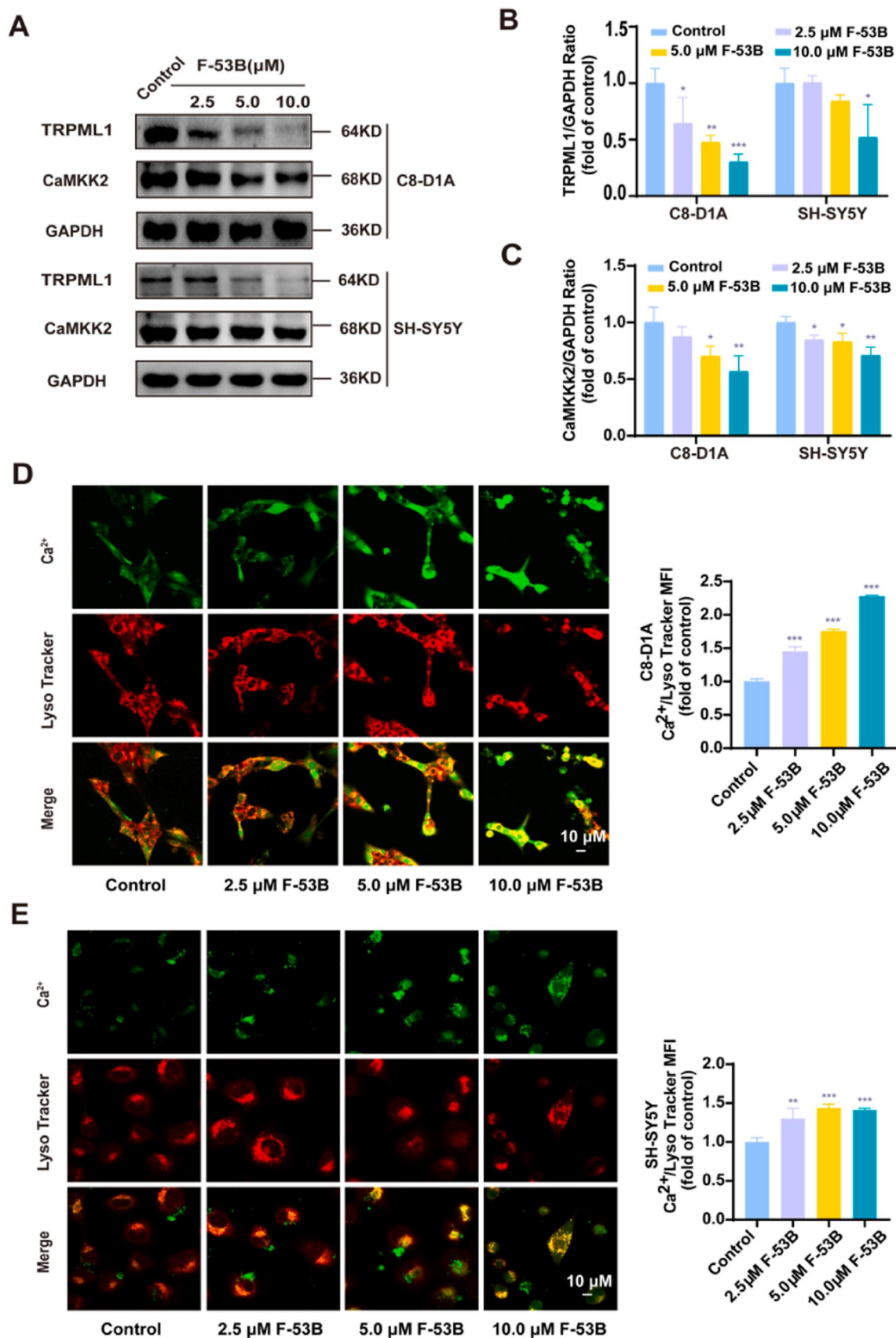


Fig. 4. F-53B exposure inhibits TRPML1 expression and reduces lysosomal Ca²⁺ release in neuronal cells. (A-C) Western blot and relative quantification of TRPML1 and CaMKK2 in C8-D1A and SH-SY5Y cells. (D) Fluorescence assay and quantitative fluorescence analysis images of lysosomal Ca²⁺ in C8-D1A cells. (E) Fluorescence assay and quantitative fluorescence analysis images of lysosomal Ca²⁺ in SH-SY5Y cells. Values represent the mean ± SD (n = 3 replicates). *P < 0.05, **P < 0.01, ***P < 0.005 compared with the control group.

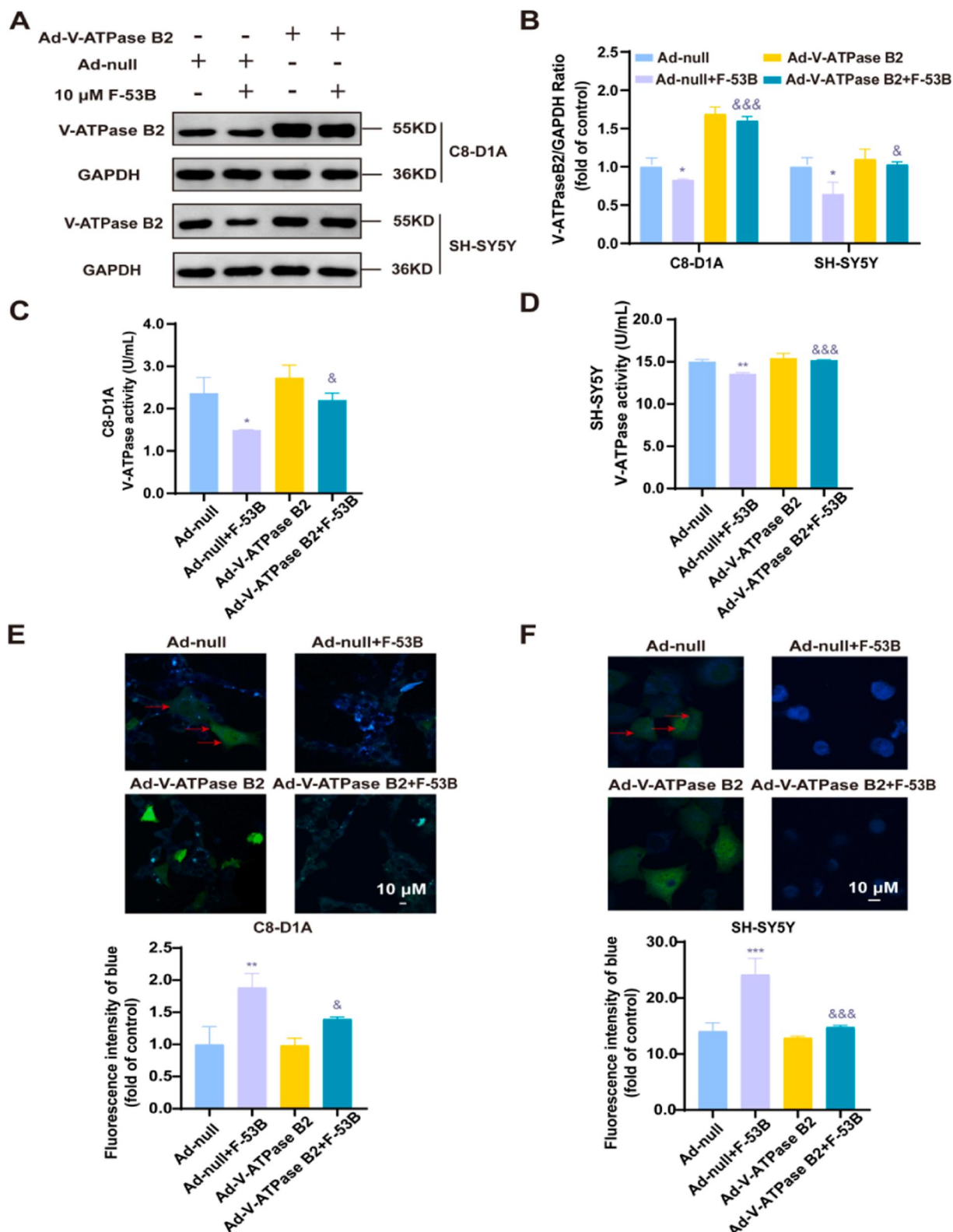


Fig. 5. V-ATPase B2 overexpression restores F-53B-induced reductions in V-ATPase B2 expression and V-ATPase activity and alleviates elevated lysosomal pH of neuronal cells. (A-B) Western blot and relative quantification of V-ATPase B2 in C8-D1A and SH-SY5Y cells after intervention with V-ATPase B2 overexpression. (C) Quantitative plot of V-ATPase complex activity in C8-D1A cells after intervention with V-ATPase B2 overexpression. (D) Quantitative plot of V-ATPase complex activity in SH-SY5Y cells after intervention with V-ATPase B2 overexpression. (E) Fluorescence assay and quantitative fluorescence analysis images of Lysosomal pH in C8-D1A cells after intervention with V-ATPase B2 overexpression. (F) Fluorescence assay and quantitative fluorescence analysis images of Lysosomal pH in SH-SY5Y cells after intervention with V-ATPase B2 overexpression. The red arrow indicated the acidic portion of the lysosomal pH. The red arrow denotes the acidic portion of the lysosomal pH. Values represent the mean \pm SD (n = 3 replicates). * P < 0.05, ** P < 0.01, *** P < 0.005 compared with the Ad-null group. & P < 0.05, && P < 0.01, &&& P < 0.001 compared with the Ad-null combined F-53B group.

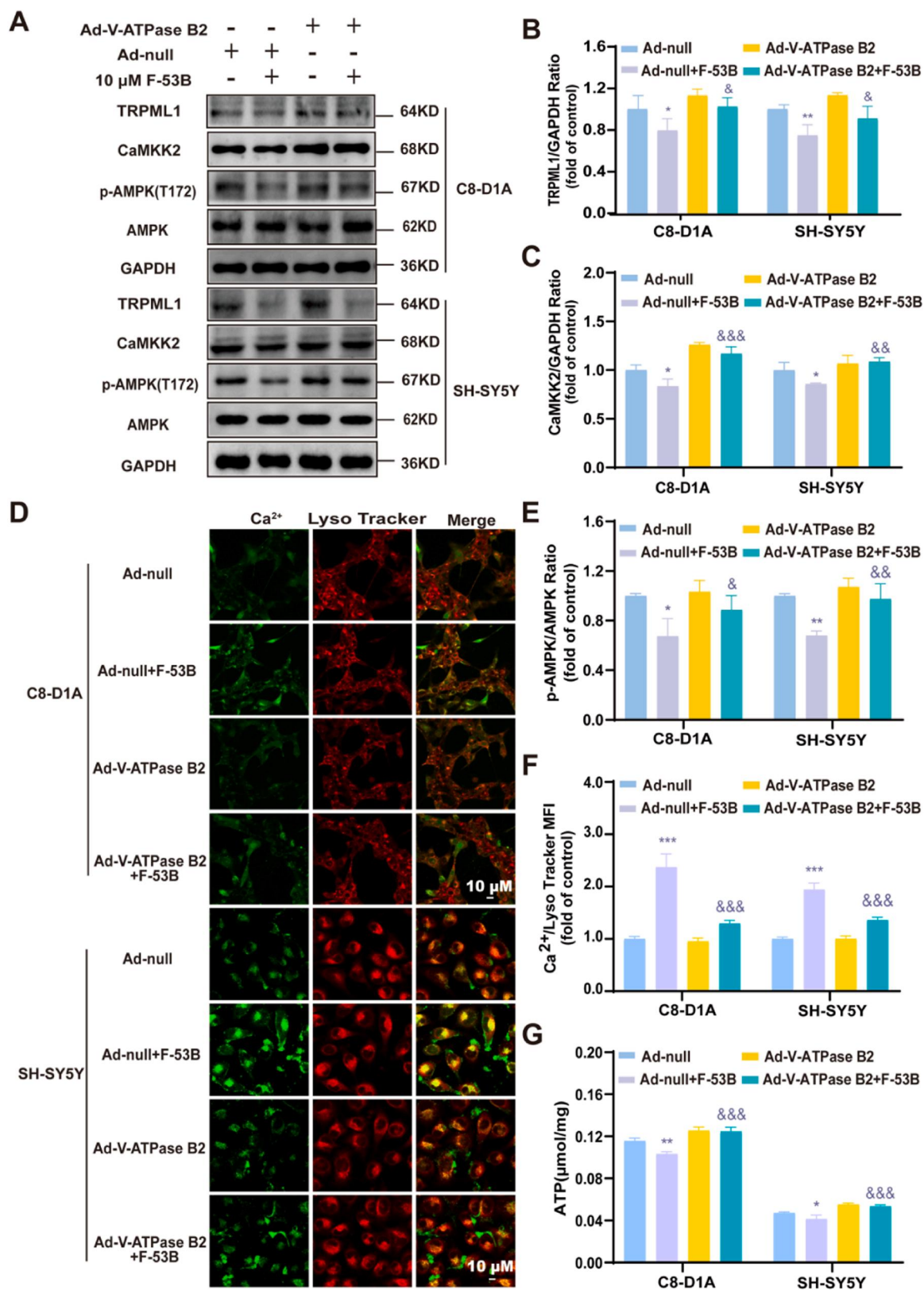


Fig. 6. V-ATPase B2 overexpression alleviates F-53B-induced TRPML1 inhibition and restores lysosomal Ca²⁺ release, AMPK activity, and ATP levels in neuronal cells. (A, B, C, E) Western blot and relative quantification of TRPML1, CaMKK2, p-AMPK and AMPK in C8-D1A and SH-SY5Y cells after intervention with V-ATPase B2 overexpression. (D, F) Fluorescence assay and quantitative fluorescence analysis images of lysosomal Ca²⁺ in C8-D1A and SH-SY5Y cells after intervention with V-ATPase B2 overexpression. (G) Plot of ATP levels in C8-D1A and SH-SY5Y cells after intervention with V-ATPase B2 overexpression. Values represent the mean \pm SD (n = 3 replicates). *P < 0.05 compare with the control group. **P < 0.01, ***P < 0.005 compared with the Ad-null group. &P < 0.05, &&P < 0.01, &&&P < 0.001 compared with the Ad-null combined F-53B group.

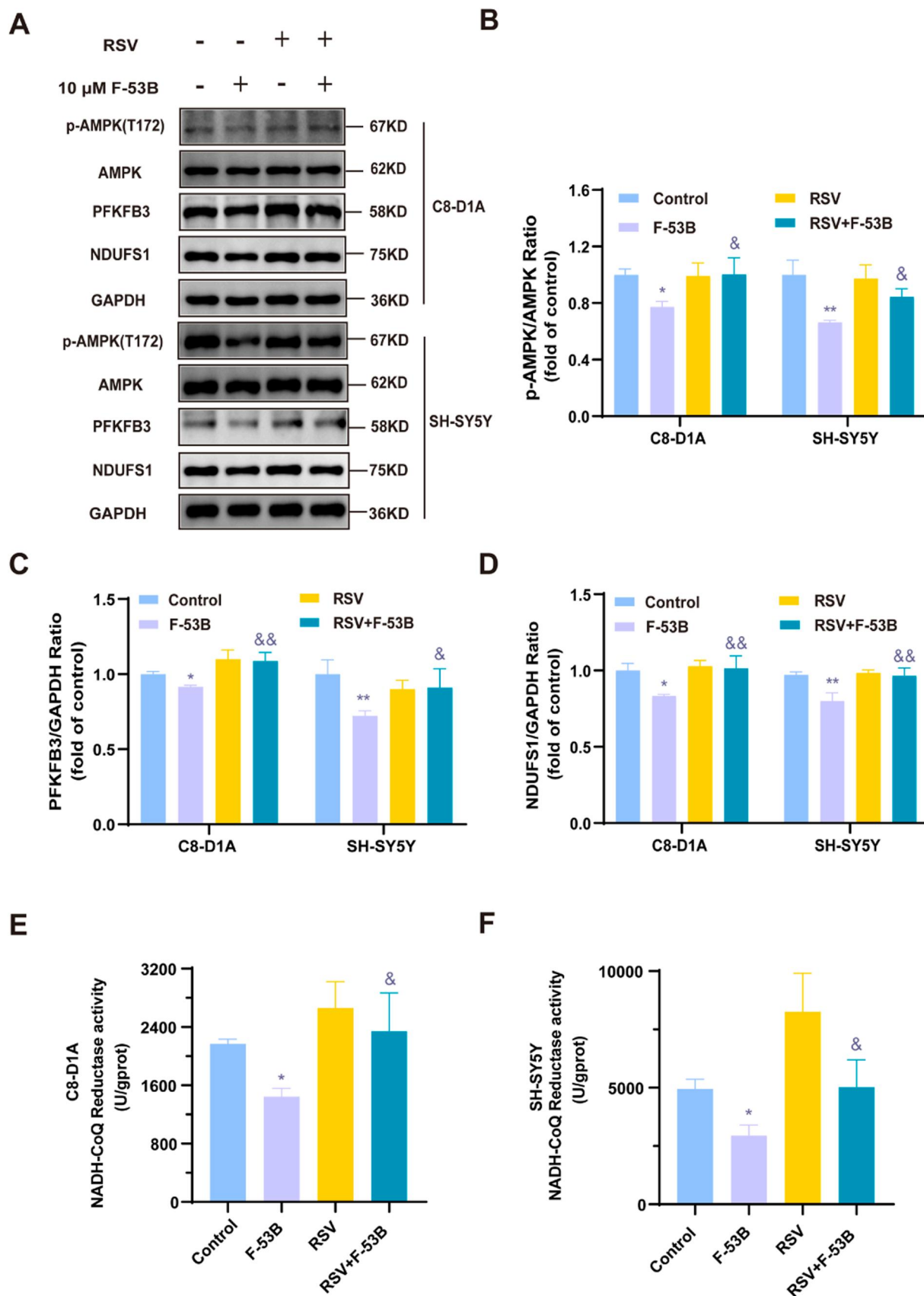


Fig. 7. RSV alleviates F-53B-induced inhibition of the expression of p-AMPK and restores cellular energy metabolic pathways in neuronal cells. (A-D) Western blot and relative quantification of p-AMPK, AMPK, PFKFB3 and NDUFS1 in C8-D1A and SH-SY5Y cells after intervention with RSV. (E) Quantitative plot of the activity of CI in C8-D1A cells after intervention with RSV. (F) Quantitative plot of the activity of CI in SH-SY5Y cells after intervention with RSV. Values represent the mean

± SD (n = 3 replicates). * $P < 0.05$, ** $P < 0.01$, *** $P < 0.005$ compared with the control group. & $P < 0.05$, && $P < 0.01$, &&& $P < 0.001$ compared with the F-53B group.

53B group compared to the F-53B group, indicating a reduction in mtROS levels (Fig. 8A-C, $P < 0.05$). Additionally, RSV significantly alleviated the reduction in MMP caused by F-53B exposure (Fig. 8D, E, $P < 0.05$). Finally, ATP levels were significantly increased in the RSV + F-53B group compared to the F-53B group, as measured by an ATP assay kit in both C8-D1A and SH-SY5Y cells (Fig. 8F, G, $P < 0.05$).

4. Discussion

In this study, we showed that F-53B increased lysosomal pH by inhibiting V-ATPase activity, inhibited TRPML1 expression and lysosomal Ca^{2+} release, attenuated CaMKK2 expression and AMPK activity, inhibited the expression of PFKFB3, NDUFS1, and CI activity, and impaired the mitochondrial function, which ultimately led to reduced ATP production and abnormal energy metabolism. Interestingly, we found that V-ATPase B2 overexpression restored V-ATPase activity inhibited by F-53B, restored lysosomal pH and Ca^{2+} release, restored AMPK activity, and ultimately restored ATP content. And RSV restored ATP content by activating AMPK to restore the expression of PFKFB3 inhibited by F-53B and the activity of CI, alleviating the decrease in the level of mitochondrial membrane potential and the increase in mitochondrial reactive oxygen species. In summary, this study confirmed the critical role of the V-ATPase-AMPK signaling axis in the neurotoxicity of F-53B.

As the central hub of cellular energy metabolism, mitochondria produce ATP through oxidative phosphorylation, providing energy to the cell. The function and health of mitochondria are, therefore, essential for maintaining cellular homeostasis. Current research has shown that the toxic effects of F-53B may be linked to mitochondrial damage [19,32]. Our findings align with this, as we observed elevated mtROS levels and decreased MMP in neuronal cells following F-53B exposure—both important indicators of mitochondrial dysfunction. These results suggest that F-53B impairs mitochondrial function.

Oxidative phosphorylation occurs within the respiratory chain complex on the inner mitochondrial membrane, with CI initiating the electron transfer process, thereby regulating the rate of oxidative phosphorylation. NDUFS1, the largest subunit of CI, plays a crucial role in this process. In this study, F-53B significantly reduced NDUFS1 protein expression, CI activity, and intracellular ATP levels in neuronal cells, indicating disruption of the oxidative phosphorylation pathway. Similar results were reported by Liu Y et al. [32], who found that a mixture of per- and polyfluoroalkyl substances (PFAS) caused mitochondrial damage and inhibited CI activity in zebrafish, leading to reduced ATP levels and energy metabolism disturbances.

In addition to oxidative phosphorylation, glycolysis also produces ATP, contributing to cellular energy homeostasis. PFKFB3 is a key regulator of glycolysis, and our study showed that F-53B inhibited PFKFB3 expression. This finding is consistent with the study by Louise J et al. [33], which demonstrated that PFOS, perfluorooctanoic acid, and perfluorononanoic acid decreased the expression of glycolysis-related genes in hepatocytes. In summary, our findings suggest that F-53B causes mitochondrial dysfunction, impairing both oxidative phosphorylation and glycolysis processes, thereby contributing to its neurotoxic effects.

AMPK serves as a crucial energy metabolism sensor in vivo, and phosphorylation of the T172 site of its α -subunit is key to its activation. Activated AMPK regulates multiple biological functions by targeting downstream pathways. For example, an animal study revealed that PFOS interferes with the beneficial hypoglycemic effects of metformin by inhibiting the AMPK pathway, thus disrupting hepatic lipid and glucose homeostasis [34]. Similarly, Yi W et al. [17] found that PFOS inhibited AMPK/mTOR/autophagy signaling, leading to hepatic lipid

accumulation. These findings confirm that PFOS can cause glucose and lipid metabolism disorders, primarily by interfering with downstream energy metabolism through the inhibition of the expression of p-AMPK. Since oxidative phosphorylation and glycolysis, both essential for energy metabolism, are regulated by AMPK, inhibition of AMPK by F-53B could similarly disrupt these processes. F-53B, a replacement for PFOS, shares a highly similar physicochemical structure and is likely to have the same disruptive effects on energy metabolism. In our study, we found that F-53B inhibits p-AMPK protein expression, further supporting the hypothesis that F-53B disrupts energy metabolism by inhibiting the expression of p-AMPK and blocking its downstream signaling pathways.

The lysosome plays a critical role in cellular metabolism, and its specific internal pH is essential for maintaining normal lysosomal function. Additionally, lysosomes are dynamic organelles responsible for Ca^{2+} storage and homeostasis *in vivo*. In an animal experiment [35], cysteine dioxygenase type 1 was found to promote CaMKK2-mediated phosphorylation of AMPK, which in turn enhanced fatty acid oxidation, an energy-producing process. Thus, CaMKK2 acts as an upstream kinase that participates in the expression of p-AMPK and regulates energy metabolism. In our study, we found that F-53B exposure inhibited CaMKK2 expression in neuronal cells, suggesting that F-53B suppresses the expression of p-AMPK by inhibiting CaMKK2. Furthermore, CaMKK2 activity is regulated by intracellular Ca^{2+} levels. Our results indicate that F-53B reduces lysosomal Ca^{2+} release into the cytoplasm, which could serve as an upstream signal to inhibit the expression of p-AMPK. Similar observations were reported by Li J et al. [20] who found that PFOS elevated lysosomal Ca^{2+} levels by disrupting TRPML1 expression, ultimately leading to insulin resistance. TRPML1, a cation channel located on the lysosomal membrane, regulates Ca^{2+} efflux from lysosomes. In our study, F-53B reduced TRPML1 protein expression, reinforcing the role of TRPML1 in controlling lysosomal Ca^{2+} levels. TRPML1 expression is strongly dependent on lysosomal pH, and its channel activity decreases as lysosomal pH increases [22]. The V-ATPase complex, located on the lysosomal membrane, maintains lysosomal pH stability by hydrolyzing ATP and transporting H^+ into the lysosome [36]. Our findings revealed that F-53B decreased V-ATPase B2 protein expression and V-ATPase complex activity, leading to an increase in lysosomal pH, suggesting that V-ATPase triggers a molecular cascade that regulates AMPK activity. Zhang C et al. [37] reported that the V-ATPase complex could activate AMPK, thereby affecting metabolic pathways. This evidence supports our experimental hypothesis that F-53B disrupts neuronal energy metabolism by inhibiting the V-ATPase-AMPK axis, ultimately reducing cellular ATP levels.

To further explore the role of the V-ATPase-AMPK signaling axis in the disruption of energy metabolism caused by F-53B, we investigated the effects of Ad-V-ATPase B2, a subunit of V-ATPase, in F-53B-treated C8-D1A and SH-SY5Y cells. Our study demonstrated that Ad-V-ATPase B2 effectively restored the diminished V-ATPase B2 expression and reduced V-ATPase activity induced by F-53B. Additionally, lysosomal pH was restored. This finding aligns with a study by Zhou X et al. [38], which demonstrated that the activation of V-ATPase promoted lysosomal pH down-regulation. Furthermore, Ad-V-ATPase B2 reversed the reduction in TRPML1 expression and lysosomal Ca^{2+} release. Collectively, our results confirmed that activation of V-ATPase alleviates both the elevation in lysosomal pH and the accumulation of lysosomal Ca^{2+} caused by F-53B. Moreover, Yoo J et al. [21] reported that lysosomal Ca^{2+} release activates the CaMKK2-AMPK-ULK1 axis and reduces fat accumulation. Similarly, we found that Ad-V-ATPase B2 restored CaMKK2 and p-AMPK protein expression, which had been inhibited by F-53B. Crucially, Ad-V-ATPase B2 mitigated the F-53B-induced reduction in ATP levels in neuronal cells, indicating that V-ATPase plays an essential upstream regulatory role in AMPK-mediated energy

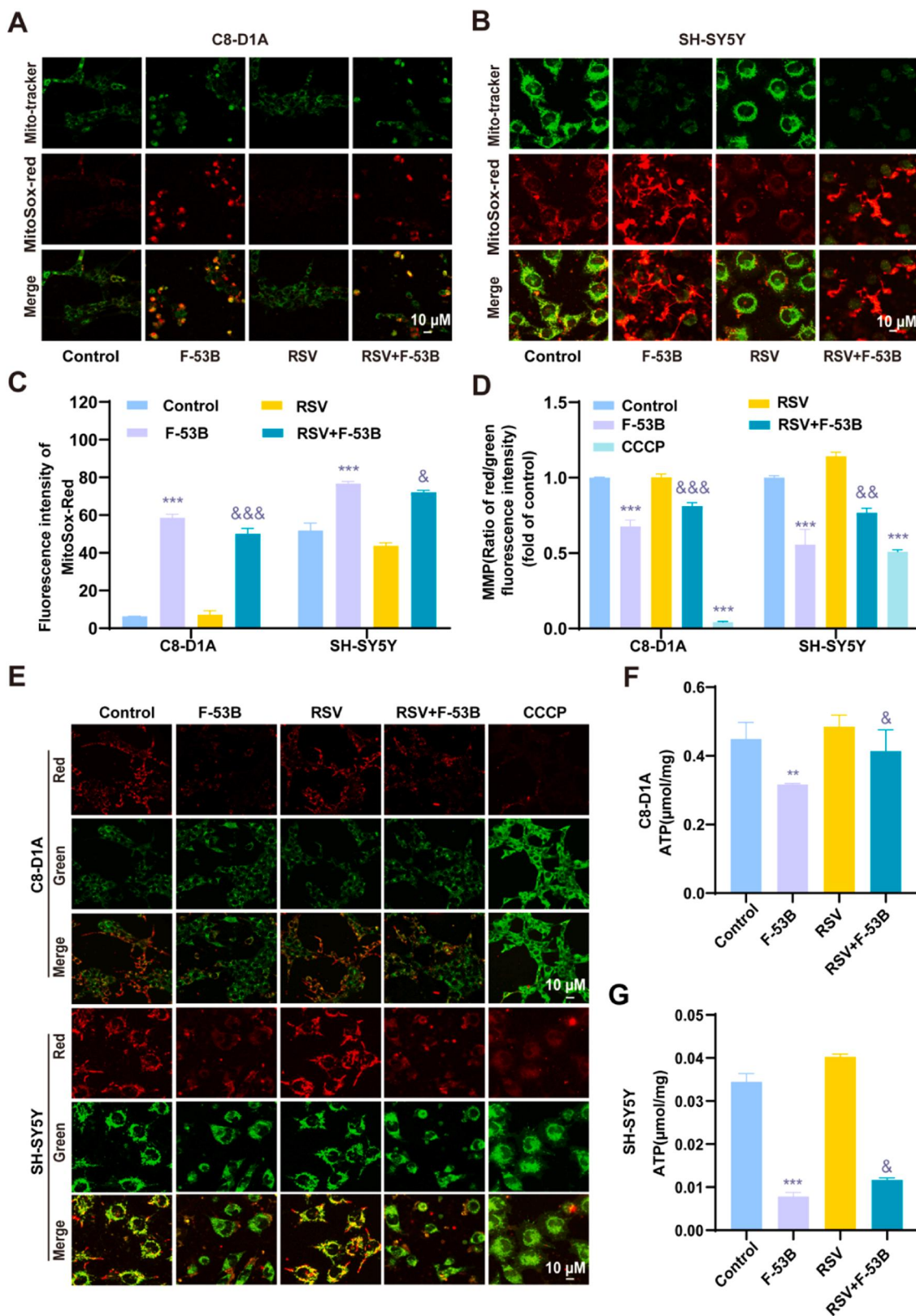


Fig. 8. RSV relieves mitochondrial damage induced by F-53B and restores cellular ATP levels in neuronal cells. (A) Representative images of mtROS in C8-D1A cells after intervention with RSV. (B) Representative images of mtROS in SH-SY5Y cells after intervention with RSV. (C) Quantitative analyses of A and B. (D) Quantitative analyses of E. (E) Representative images of MMP in C8-D1A and SH-SY5Y cells after intervention with RSV. Red signals indicate JC-1 aggregate, green signals indicate JC-1 monomer, and CCCP is used as a positive control. (F) Plot of ATP levels in C8-D1A cells after intervention with RSV. (G) Plot of ATP levels in SH-SY5Y cells after intervention with RSV. Values represent the mean \pm SD (n = 3 replicates). * $P < 0.05$, ** $P < 0.01$, *** $P < 0.005$ compared with the control group. & $P < 0.05$, && $P < 0.01$, &&& $P < 0.001$ compared with the F-53B group.

metabolism.

In addition, we further investigated the role of AMPK in F-53B-treated C8-D1A and SH-SY5Y cells by utilizing RSV, which has a high utility value, in order to activate AMPK. Current research suggests that RSV activates AMPK, thereby protecting mitochondrial function and increasing ATP levels[39,40]. A previous study revealed that RSV had beneficial effects on congenital deficiencies in mitochondrial complexes I and V, stimulating mitochondrial function in an AMPK-dependent manner[41]. Similarly, our findings showed that RSV intervention restored NDUFS1 protein expression and CI activity, both of which were inhibited by F-53B. RSV also reduced mtROS levels, restored MMP, and increased ATP levels. Furthermore, we found that RSV alleviated the inhibition of p-AMPK and PFKFB3 expression. Bao Y et al.[42] also showed that AMPK activation promotes PFKFB3 expression, thereby enhancing glycolysis. RSV's ability to promote the expression of p-AMPK, alleviate the F-53B-induced inhibition of energy metabolism pathways, repair mitochondrial damage, and restore cellular ATP levels confirms its role in mitigating impaired energy metabolism in neuronal cells, as expected. Thus, while Ad-V-ATPase B2 indirectly activated AMPK, RSV directly activated AMPK, attenuated the inhibition of the V-ATPase-AMPK axis caused by F-53B, alleviated energy metabolism disorders, and restored ATP levels.

5. Conclusion

Our findings demonstrated that F-53B inhibited V-ATPase activity, elevated lysosomal pH, and led to lysosomal Ca^{2+} accumulation, which subsequently blocked the expression of p-AMPK and its downstream signaling pathways by reducing CaMKK2 expression. This regulatory mechanism disrupted the V-ATPase-AMPK signaling axis, causing severe energy metabolism dysfunction in neuronal cells and reducing ATP production. Notably, interventions with Ad-V-ATPase B2 and RSV significantly mitigated F-53B-induced neurocytotoxicity. These findings provide new insights into the neurotoxic mechanisms of F-53B and suggest potential targets for future neuroprotective strategies aimed at modulating the V-ATPase-AMPK signaling axis, offering both scientific and practical significance.

Environmental Implications

F-53B, as a substitute for perfluorooctane sulfonate, is considered a new type of environmental organic pollutant. More research has found that F-53B is widely present in environmental and biological samples, indicating that its toxicity is comparable or similar to perfluorooctane sulfonate, and the hazards of F-53B should be taken seriously. Our research found that F-53B interferes with the energy metabolism process of nerve cells. Meanwhile, interventions with Ad-V-ATPase B2 and resveratrol can alleviate this adverse reaction.

Our research results are of great significance to the environment and health, so I would like to submit them to your journal.

CRedit authorship contribution statement

Yue Zhang: Methodology, Conceptualization. **Qiang Niu:** Writing – review & editing. **Xueman Ding:** Writing – original draft, Data curation. **Tingting Li:** Writing – original draft, Data curation. **Chun Wang:** Supervision. **Wenqi Qin:** Supervision. **Mulatibieke Keerman:** Validation, Software. **Runjiang Ma:** Visualization, Investigation. **Li Liu:** Visualization, Investigation. **Chulin Yan:** Supervision. **Jingjing Zhang:** Visualization, Investigation.

Declaration of Competing Interest

The authors declare that they have no known competing financial interests or personal relationships that could have appeared to influence the work reported in this paper.

Acknowledgments

This study was supported by grants from the National Natural Science Foundation of China (Grant Nos. 82360671 and 82060580), the Bingtuan Program of Science and Technology Innovation (Grant No. 2021CB046), Shihezi University independently funded and supported university-level scientific research projects (No. ZZZC2023027), as well as the Shihezi University International Science and Technology Cooperation Promotion Programme Project (No. GJHZ202308). Graphical abstract was created using Figdraw.

Appendix A. Supporting information

Supplementary data associated with this article can be found in the online version at [doi:10.1016/j.jhazmat.2025.137111](https://doi.org/10.1016/j.jhazmat.2025.137111).

Data Availability

Data will be made available on request.

References

- [1] Wang, T., Wang, Y., Liao, C., et al., 2009. Perspectives on the inclusion of perfluorooctane sulfonate into the stockholm convention on persistent organic pollutants [J]. *Environmental Science & Technology* 43 (14), 5171–5175.
- [2] Feng, Y., Wu, H., Feng, L., et al., 2024. Maternal F-53B exposure during pregnancy and lactation induced glucolipid metabolism disorders and adverse pregnancy outcomes by disturbing gut microbiota in mice [J]. *Science of the total environment* 915, 170130.
- [3] Pan, Y., Zhang, H., Cui, Q., et al., 2018. Worldwide distribution of novel perfluoroether carboxylic and sulfonic acids in surface water [J]. *Environmental Science & Technology* 52 (14), 7621–7629.
- [4] Ruan, T., Lin, Y., Wang, T., et al., 2015. Identification of novel polyfluorinated ether sulfonates as PFOS alternatives in municipal sewage sludge in China [J]. *Environmental Science & Technology* 49 (11), 6519–6527.
- [5] Liu, W., Qin, H., Li, J., et al., 2017. Atmospheric chlorinated polyfluorinated ether sulfonate and ionic perfluoroalkyl acids in 2006 to 2014 in Dalian, China [J]. *Environmental Toxicology and Chemistry* 36 (10), 2581–2586.
- [6] Wang, W., Lee, J., Oh, J., et al., 2021. Per- and polyfluoroalkyl substances and their alternatives in black-tailed gull (*Larus crassirostris*) eggs from South Korea islands during 2012–2018 [J]. *Journal of Hazardous Materials* 411, 125036.
- [7] Gebbink, W.A., Bossi, R., Rigét, F.F., et al., 2016. Observation of emerging per- and polyfluoroalkyl substances (PFASs) in Greenland marine mammals [J]. *Chemosphere* 144, 2384–2391.
- [8] Wang, S., Huang, J., Yang, Y., et al., 2013. First Report of a Chinese PFOS Alternative Overlooked for 30 Years: Its Toxicity, Persistence, and Presence in the Environment [J]. *Environmental Science & Technology* 47 (18), 10163–10170.
- [9] He, Y., Lv, D., Li, C., et al., 2022. Human exposure to F-53B in China and the evaluation of its potential toxicity: An overview [J]. *Environment International* 161, 107108.
- [10] Shi, Y., Vestergren, R., Xu, L., et al., 2016. Human exposure and elimination kinetics of chlorinated polyfluoroalkyl ether sulfonic acids (Cl-PFESAs) [J]. *Environmental Science & Technology* 50 (5), 2396–2404.
- [11] Wang, J., Pan, Y., Cui, Q., et al., 2018. Penetration of PFASs across the blood cerebrospinal fluid barrier and its determinants in humans [J]. *Environmental Science & Technology* 52 (22), 13553–13561.
- [12] Li, J., Su, X., Zhou, Y., et al., 2024. Association between prenatal exposure to per- and polyfluoroalkyl substances and infant anthropometry: A prospective cohort study [J]. *International Journal of Hygiene and Environmental Health* 257, 114339.
- [13] Yin, N., Yang, R., Liang, S., et al., 2018. Evaluation of the early developmental neural toxicity of F-53B, as compared to PFOS, with an in vitro mouse stem cell differentiation model [J]. *Chemosphere* 204, 109–118.
- [14] Cheng, X., Huang, N., Sheng, Z., 2022. Programming axonal mitochondrial maintenance and bioenergetics in neurodegeneration and regeneration [J]. *Neuron* 110 (12), 1899–1923.
- [15] Trefts, E., Shaw, R.J., 2021. AMPK: restoring metabolic homeostasis over space and time [J]. *Molecular Cell* 81 (18), 3677–3690.
- [16] Vercellino, I., Sazanov, L.A., 2022. The assembly, regulation and function of the mitochondrial respiratory chain [J]. *Nature reviews. Molecular cell Biology* 23 (2), 141–161.
- [17] Yi, W., Shi, J., Wang, L., et al., 2024. Maternal PFOS exposure in mice induces hepatic lipid accumulation and inflammation in adult female offspring: involvement of microbiome-gut-liver axis and autophagy [J]. *Journal of Hazardous Materials* 470, 134177.
- [18] Hofmann, A., Mishra, J.S., Yadav, P., et al., 2023. PFOS Impairs Mitochondrial Biogenesis and Dynamics and Reduces Oxygen Consumption in Human Trophoblasts [J]. *Journal of Environmental Science and Public Health* 7 (4), 164–175.

- [19] Nie, P., Lan, Y., You, T., et al., 2024. F-53B mediated ROS affects uterine development in rats during puberty by inducing apoptosis [J]. *Ecotoxicology and Environmental Safety* 277, 116399.
- [20] Li, J., Ma, Y., Qiu, T., et al., 2024. Autophagy-dependent lysosomal calcium overload and the ATP5B-regulated lysosomes-mitochondria calcium transmission induce liver insulin resistance under perfluorooctane sulfonate exposure [J]. *Metabolism: Clinical and Experimental* 120, 154798.
- [21] Yoo, J., Jeong, I., Ahn, K.J., et al., 2021. Fenofibrate, a PPAR α agonist, reduces hepatic fat accumulation through the upregulation of TFEB-mediated lipophagy [J]. *Metabolism: Clinical and Experimental* 120, 154798.
- [22] Prat Castro, S., Kudrina, V., Jašlan, D., et al., 2022. Neurodegenerative Lysosomal Storage Disorders: TPC2 Comes to the Rescue! [J]. *Cells* 11 (18).
- [23] Yao, X., Liu, Y., Mao, M., et al., 2024. Calorie restriction mimetic, resveratrol, attenuates hepatic ischemia and reperfusion injury through enhancing efferocytosis of macrophages via AMPK/STAT3/S1PR1 pathway [J]. *The Journal of Nutritional Biochemistry* 126, 109587.
- [24] Timmers, S., Konings, E., Bilet, L., et al., 2011. Calorie restriction-like effects of 30 days of resveratrol supplementation on energy metabolism and metabolic profile in obese humans [J]. *Cell Metabolism* 14 (5), 612–622.
- [25] Wang, H., Wang, Z., Ding, Y., et al., 2018. Endoplasmic reticulum stress regulates oxygen-glucose deprivation-induced parthanatos in human SH-SY5Y cells via improvement of intracellular ROS [J]. *CNS Neuroscience & Therapeutics* 24 (1), 29–38.
- [26] Lopez-Suarez, L., Awabdh, S.A., Coumoul, X., et al., 2022. The SH-SY5Y human neuroblastoma cell line, a relevant in vitro cell model for investigating neurotoxicology in human: focus on organic pollutants [J]. *Neurotoxicology* 92, 131–155.
- [27] Herrera Moro Chao, D., Kirchner, M.K., Pham, C., et al., 2022. Hypothalamic astrocytes control systemic glucose metabolism and energy balance [J]. *Cell Metabolism* 34 (10), 1532–1547.
- [28] Chen, Z., Yuan, Z., Yang, S., et al., 2023. Brain energy metabolism: astrocytes in neurodegenerative diseases [J]. *CNS Neuroscience & Therapeutics* 29 (1), 24–36.
- [29] Chiang, M., Nicol, C.J.B., Lo, S., et al., 2022. Resveratrol mitigates oxygen and glucose deprivation-induced inflammation, NLRP3 inflammasome, and oxidative stress in 3D neuronal culture [J]. *International Journal of Molecular Sciences* 23 (19).
- [30] Xie, Z., Ying, Q., Luo, H., et al., 2023. Resveratrol Alleviates Retinal Ischemia-Reperfusion Injury by Inhibiting the NLRP3/Gasdermin D/Caspase-1/Interleukin-1 β Pyroptosis Pathway [J]. *Investigative Ophthalmology & Visual Science* 64 (15), 28.
- [31] Sun, Q., Kang, R., Chen, K., et al., 2021. Sirtuin 3 is required for the protective effect of Resveratrol on Manganese-induced disruption of mitochondrial biogenesis in primary cultured neurons [J]. *Journal of Neurochemistry* 156 (1), 121–135.
- [32] Liu, Y., Liu, S., Huang, J., et al., 2023. Mitochondrial dysfunction in metabolic disorders induced by per- and polyfluoroalkyl substance mixtures in zebrafish larvae [J]. *Environment International* 176, 107977.
- [33] Louise, J., Rijkers, D., Stoop, G., et al., 2020. Perfluorooctanoic acid (PFOA), perfluorooctane sulfonic acid (PFOS), and perfluorononanoic acid (PFNA) increase triglyceride levels and decrease cholesterogenic gene expression in human HepaRG liver cells [J]. *Archives of Toxicology* 94 (9), 3137–3155.
- [34] Salter, D.M., Wei, W., Nahar, P.P., et al., 2021. Perfluorooctanesulfonic Acid (PFOS) Thwarts the Beneficial Effects of Calorie Restriction and Metformin [J]. *Toxicological Sciences: an Official Journal of the Society of Toxicology* 182 (1), 82–95.
- [35] Chen, M., Zhu, J., Mu, W., et al., 2023. Cdo1-Camkk2-AMPK axis confers the protective effects of exercise against NAFLD in mice [J]. *Nature Communications* 14 (1), 8391.
- [36] Colacurcio, D.J., Nixon, R.A., 2016. Disorders of lysosomal acidification-The emerging role of v-ATPase in aging and neurodegenerative disease [J]. *Ageing Research Reviews* 32, 75–88.
- [37] Zhang, C., Jiang, B., Li, M., et al., 2014. The lysosomal v-ATPase-Ragulator complex is a common activator for AMPK and mTORC1, acting as a switch between catabolism and anabolism [J]. *Cell Metabolism* 20 (3), 526–540.
- [38] Zhou, X., Zhao, S., Liu, T., et al., 2022. Schisandrol A protects AGES-induced neuronal cells death by allosterically targeting ATP6V0d1 subunit of V-ATPase [J]. *Acta Pharmaceutica Sinica. B* 12 (10), 3843–3860.
- [39] Shaito, A., Al-Mansoor, M., Ahmad, S.M.S., et al., 2023. Resveratrol-mediated regulation of mitochondria biogenesis-associated pathways in neurodegenerative diseases: molecular insights and potential therapeutic applications [J]. *Current Neuropharmacology* 21 (5), 1184–1201.
- [40] Zhu, Z., Zhao, H., Cui, H., et al., 2023. Resveratrol improves the frozen-thawed ram sperm quality [J]. *Animals: an Open Access Journal from MDPI*, 13 (24).
- [41] Lopes Costa, A., Le Bachelier, C., Mathieu, L., et al., 2014. Beneficial effects of resveratrol on respiratory chain defects in patients' fibroblasts involve estrogen receptor and estrogen-related receptor alpha signaling [J]. *Human Molecular Genetics* 23 (8), 2106–2119.
- [42] Bao, Y., Xiao, J., Weng, Z., et al., 2020. A phenolic glycoside from *Moringa oleifera* Lam. improves the carbohydrate and lipid metabolisms through AMPK in db/db mice [J]. *Food Chemistry* 311, 125948.